



On the question of fractal packing structure in metallic glasses

Jun Ding^a, Mark Asta^{a,b,1}, and Robert O. Ritchie^{a,b,1}

^aMaterials Sciences Division, Lawrence Berkeley National Laboratory, Berkeley, CA 94720; and ^bDepartment of Materials Science and Engineering, University of California, Berkeley, CA 94720

Edited by Andrea J. Liu, University of Pennsylvania, Philadelphia, PA, and approved June 30, 2017 (received for review April 6, 2017)

This work addresses the long-standing debate over fractal models of packing structure in metallic glasses (MGs). Through detailed fractal and percolation analyses of MG structures, derived from simulations spanning a range of compositions and quenching rates, we conclude that there is no fractal atomic-level structure associated with the packing of all atoms or solute-centered clusters. The results are in contradiction with conclusions derived from previous studies based on analyses of shifts in radial distribution function and structure factor peaks associated with volume changes induced by pressure and compositional variations. The interpretation of such shifts is shown to be challenged by the heterogeneous nature of MG structure and deformation at the atomic scale. Moreover, our analysis in the present work illustrates clearly the percolation theory applied to MGs, for example, the percolation threshold and characteristics of percolation clusters formed by subsets of atoms, which can have important consequences for structure–property relationships in these amorphous materials.

metallic glass | fractal structure | percolation cluster | dimensionality | inhomogeneous deformation

Metallic glasses (MGs) are of significant current interest because of their unique combination of mechanical properties (1–7). Although it is generally understood that these properties arise from the nature of the MG structure, the understanding of this structure, spanning atomic to medium-range scales, remains incomplete. In recent years, fractal concepts have been introduced (e.g., refs. 8–10) to describe the structure of MGs: that is, based on self-similar patterns of packing structure repeated at different length scales (11). These models have been invoked to explain (8, 9, 12–14) widely observed noncubic power laws (D) correlating positions of the first sharp diffraction peak, q , or the first peak of radial distribution functions (RDFs), r , with the average atomic volume, V (or bulk atomic density, $\rho = 1/V$), that is:

$$V = 1/\rho \sim r^D \text{ or } (1/q)^D. \quad [1]$$

Exponents of $D \approx 2.5$ or 2.3 have been measured in MGs, or the metallic melts from which they are derived based on scattering experiments and computer simulations (8, 9, 12–14), in which the changes in atomic volume V have been investigated through applications of hydrostatic pressure or compositional variations. These measurements, which are in contrast to the situation for crystalline metals and alloys, where the scaling in Eq. 1 is characterized by $D = 3$, have led to the proposal of two distinct fractal models for the structure of MGs, associated with the packing of local clusters or atoms (see illustration of atomic configuration in Fig. 1A). In the first such model (9), it was proposed that MGs are composed of solute (minority atom)-centered clusters that are arranged on medium-range scales in a fractal manner. This description has been the subject of debate in the literature (7, 14, 15), and more recently Chen et al. (8, 10) proposed a description in which the individual atoms of MGs are packed according to a special class of fractal models, namely, a percolation cluster. This latter description serves to solve the puzzle of how MGs can simultaneously exhibit fractal structure yet remain fully dense; the fractal behavior, $D \approx 2.5$, was reported to

arise at short-range scales, whereas the structure is homogeneous (i.e., $D = 3$) at larger length scales.

In what follows, we present a detailed analysis of these fractal models of the atomic structure in a variety of MGs derived by computer simulation, as well as extracted from experimental data taken from the literature. Structural analyses have been conducted that are based on established methodologies characterizing the scaling of the distance-dependent atomic mass/density distribution, as well as percolation theory. The results establish that there is no fractal packing structure, considering the packing of either all of the atoms or solute-centered clusters in the MG systems analyzed. The findings are thus at odds with the models summarized above, and we demonstrate that conclusions concerning fractal dimensionality derived from the scaling relations in Eq. 1, that is, based on measurements of the changes in the RDFs and structure factor peaks induced by pressure and compositional variations, can be misleading due to the heterogeneous nature of the MG structure and its nonaffine deformation. The current analysis establishes that percolation clusters emerge when considering a small subset of the atoms drawn at random from the MG structures, and we discuss how the presence of such percolation clusters may have important implications for properties including the glass transition and mechanical deformation.

Fractal Dimension and Percolation Analysis of MGs

We use large-scale molecular-dynamics (MD) simulations (16) to prepare 12 distinct MG samples, listed in Table 1, which span a wide range of compositions and cooling rates (defined in *Methods*). These include binary, ternary, as well as monatomic MGs (Table 1), including the $\text{Cu}_{46}\text{Zr}_{54}$ and $\text{Ni}_{80}\text{Al}_{20}$ systems considered in previous simulation studies (8). In the present work, each sample is larger than those considered in previous simulation studies of fractal

Significance

Our work clearly demonstrates a lack of fractal structure in metallic glasses, considering the packing of all atoms or solute-centered clusters. This finding clarifies the long-standing debate over the packing structure of metallic glasses from the perspective of fractal models; it is thus of significance for the community of researchers working with amorphous solids. Moreover, our percolation analysis of metallic glasses, revealing their cluster structure and percolation threshold, provides an important and powerful theoretical framework to describe the properties of amorphous alloys, such as the glass transition and mechanical deformation.

Author contributions: J.D., M.A., and R.O.R. designed research; J.D. performed research; J.D. contributed new reagents/analytic tools; J.D., M.A., and R.O.R. analyzed data; and J.D., M.A., and R.O.R. wrote the paper.

The authors declare no conflict of interest.

This article is a PNAS Direct Submission.

¹To whom correspondence may be addressed. Email: roritche@lbl.gov or mdasta@berkeley.edu.

This article contains supporting information online at www.pnas.org/lookup/suppl/doi:10.1073/pnas.1705723114/-DCSupplemental.

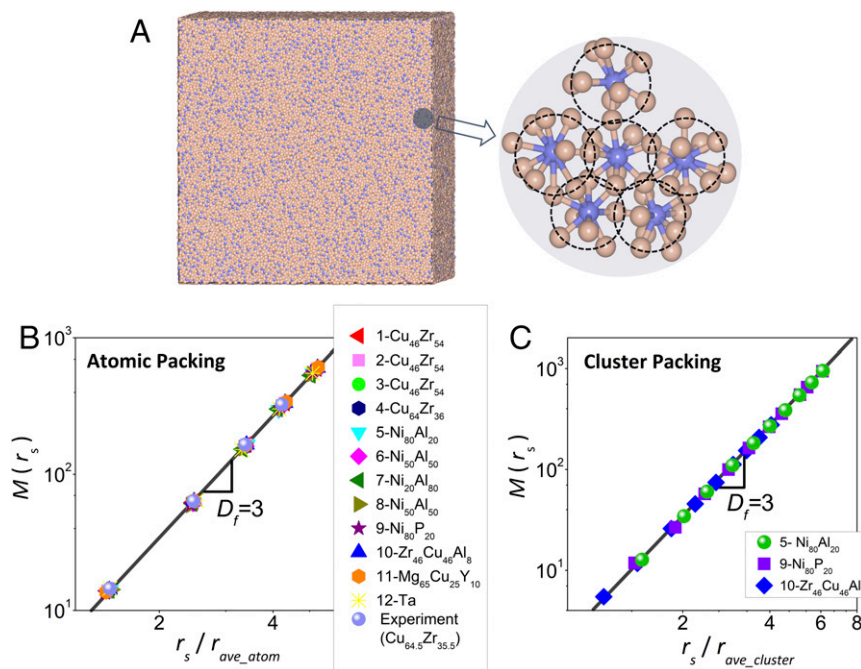


Fig. 1. Universal dimensionality for MGs. (A) Atomic configuration of the MD-simulated Ni₈₀P₂₀ MG (sample 9 in Table 1); pink and blue balls represent Ni and P atoms, respectively; the magnified view (Right) illustrates the packing of solute (P)-centered clusters (delineated by black dashed circles), exhibiting fivefold symmetry; only the Ni-P pairs are plotted. B and C show the analysis of distance-dependent mass distribution (Eq. 2) for the packing of all atoms and solute atoms (reflecting solute-centered clusters), respectively, among MGs listed in Table 1. r_s is the radius of a region within the material, centered on an atom or a solute species, and $M(r_s)$ is the mass [i.e., (B) number of atoms or (C) number of solute atoms] within r_s . The solid lines are the best fit of all of the data, with a slope of dimension $D_f = 3$. For the x axis in B and C, r_s is normalized by the average atomic spacing (i.e., r_{ave_atom}) and average solute-atom spacing (i.e., $r_{ave_cluster}$), respectively, as defined in the text. Experimental data of the Cu_{64.5}Zr_{35.5} MG, extracted from ref. 18, are also plotted in B.

structure, with more than 1 million atoms, to produce smoother RDFs with higher resolution (Fig. S1).

From the simulated MG structures, we implement a classical analysis of fractal structure by analyzing the power-law scaling of the mass distribution (11, 17):

$$M(r_s) \sim r_s^{D_f}, \quad [2]$$

where r_s is the radius of a region within the material, $M(r_s)$ is the mass (i.e., number of atoms or solute atoms) within r_s , and D_f is the fractal dimension (examples of this analysis, for simple-cubic and face-centered cubic crystals, are shown in Fig. S2). Theoretically, for a 3D material, noncubic values for D_f indicate fractal structure (11, 17). Fig. 1B shows the mass distribution analysis for the packing of all of the atoms (independent of type), among all of the 12 MG

samples studied in this work, as well as an experimental sample of Cu_{64.5}Zr_{35.5} MG (extracted from ref. 18). The slope is found to be consistent with $D_f = 3$ for power-law scaling between $M(r_s)$ and r_s , where r_s is chosen as the radial distance to the local minima of the RDFs separating two nearby atomic shells (Fig. S1). If r_s is normalized by the corresponding average atomic spacing $r_{ave_atom} = V^{1/3}$ (V is the average atomic volume), the scaling between $M(r_s)$ and r_s/r_{ave_atom} for all MGs collapse on a line with $D_f = 3$, as shown in Fig. 1B. Thus, we conclude that, in these MGs, there is no suggestion of a slope change to noncubic values of D_f for values of the radii down to that corresponding to the nearest-neighbor shell, which is consistent with our percolation analysis below, for the correlation length of percolation clusters for the packing of all atoms in MGs.

Percolation analysis provides a complementary framework for analyzing the fractal nature of the atomic structure. In this approach,

Table 1. List of large-scale model MG systems studied in the present work

No.	Composition	No. of atoms	Cooling rate, K/s	Sample size, nm	Interatomic potential
1	Cu ₄₆ Zr ₅₄	1,024,000	10 ¹⁰	26.421	Cheng et al. (31)
2	Cu ₄₆ Zr ₅₄	1,024,000	10 ¹²	26.431	Cheng et al. (31)
3	Cu ₄₆ Zr ₅₄	1,024,000	10 ¹²	26.422	Mendelev et al. (18)
4	Cu ₆₄ Zr ₃₆	1,250,000	10 ¹²	27.146	Cheng et al. (31)
5	Ni ₈₀ Al ₂₀	1,024,000	10 ¹²	22.605	Pun and Mishin (32)
6	Ni ₅₀ Al ₅₀	1,024,000	10 ¹²	23.311	Pun and Mishin (32)
7	Ni ₂₀ Al ₈₀	1,024,000	10 ¹²	24.889	Pun and Mishin (32)
8	Ni ₅₀ Al ₅₀	1,024,000	10 ¹²	23.591	Mishin et al. (33)
9	Ni ₈₀ P ₂₀	1,024,000	10 ¹²	22.503	Sheng et al. (34)
10	Zr ₄₆ Cu ₄₆ Al ₈	1,024,000	10 ¹²	26.125	Cheng et al. (31)
11	Mg ₆₅ Cu ₂₅ Y ₁₀	1,024,000	10 ¹²	27.781	Ding et al. (35)
12	Ta	1,024,000	10 ¹³	26.861	Zhong et al. (36)

For each system, we indicate the composition, the number of atoms, cooling rates, sample size, and the classical interatomic potential models used to describe the interatomic interactions.

a subgroup of atoms within a given MG sample is generated by randomly selecting atoms with an occupation probability p (*Methods*). The correlation length ξ of percolation clusters, which depends on the value of p and reflects their characteristic size, can then be computed from these randomly sampled structures. The dependence of the resulting correlation lengths on p can be used to evaluate the structure of percolation clusters in metallic glasses. We use such a site percolation analysis using simulated MGs of large-scale samples (containing ~ 27 million atoms), to minimize finite-size scaling effects. Fig. 2 *A* and *B* shows examples of slices illustrating the associated percolation clusters for a $\text{Cu}_{46}\text{Zr}_{54}$ MG sample, generated with occupation probabilities of $p = 0.192$ and 0.198 , respectively. The percolation threshold, p_c , is measured as $p_c \approx 0.1864$, as the critical value of occupation probability that percolation clusters are formed (Fig. S3). Only the atoms within the percolated clusters of MG configurations are plotted in Fig. 2 *A* and *B*, and the characteristic size of the “pores” (empty space) is seen to grow with decreasing values of p .

One definition of the correlation length, described in refs. 19 and 20, follows from the following scaling relations for the mass and density:

$$M(r_s) \propto \begin{cases} r_s^{D_f}, & r_s \ll \xi' \\ r_s^3, & r_s \gg \xi' \end{cases} \quad [3]$$

and

$$\rho(r_s) \propto \frac{M(r_s)}{r_s^3} \propto \begin{cases} r_s^{D_f-3}, & r_s \ll \xi' \\ 1, & r_s \gg \xi' \end{cases} \quad [4]$$

From this definition, as illustrated in Fig. 2*C*, the correlation length ξ' can be determined from the simulated samples as a crossover for the scaling with radial distance r of the density of

the percolation clusters, $\rho(r_s)$. The negative slope at smaller r_s corresponds to the power of $(D_f - 3)$, whereas at larger length scales the plot is horizontal slope, consistent with the scaling for large r in Eq. 4; the corresponding crossover denotes the correlation length ξ' . In Fig. 2*D*, the dependence of the calculated values of ξ' on p is presented, along with similar data for an alternative correlation length, ξ'' , defined in ref. 19 as follows:

$$(\xi'')^2 = \frac{2\Sigma R_s^2 s^2 n_s}{\Sigma s^2 n_s}, \quad [5]$$

where R_s , s , and n_s are the gyration radius, number of atoms, and cluster population, respectively, of nonpercolated clusters (19). The correlation lengths ξ' and ξ'' in Fig. 2*D* follow the power-law scaling:

$$\xi', \xi'' \propto |p - p_c|^{-\nu}, \quad [6]$$

where $\nu \approx 0.875$ (11, 19) is a critical exponent describing the dependence of the correlation length on p associated with the percolation transition. This critical exponent is a universal quantity only depending on the dimension of the lattice (11). As shown from the extrapolation of this relation in Fig. 2*D*, for correlation lengths to take values corresponding to the average atomic spacing (horizontal dashed line in Fig. 2*D*), a small fraction ($p = \sim 0.28-0.35$) of atoms in a MG would need to be considered, rather than the packing of all atoms ($p = 1$). The results of this analysis are thus consistent with conclusions derived from Fig. 1*B*, namely, that there is no fractal scaling for the packing of all of the atoms, down to the scale of the atomic spacing. Additional results from the percolation analyses, including the density of the percolation cluster, as well as the percolation threshold for MGs, are presented in Fig. S3.

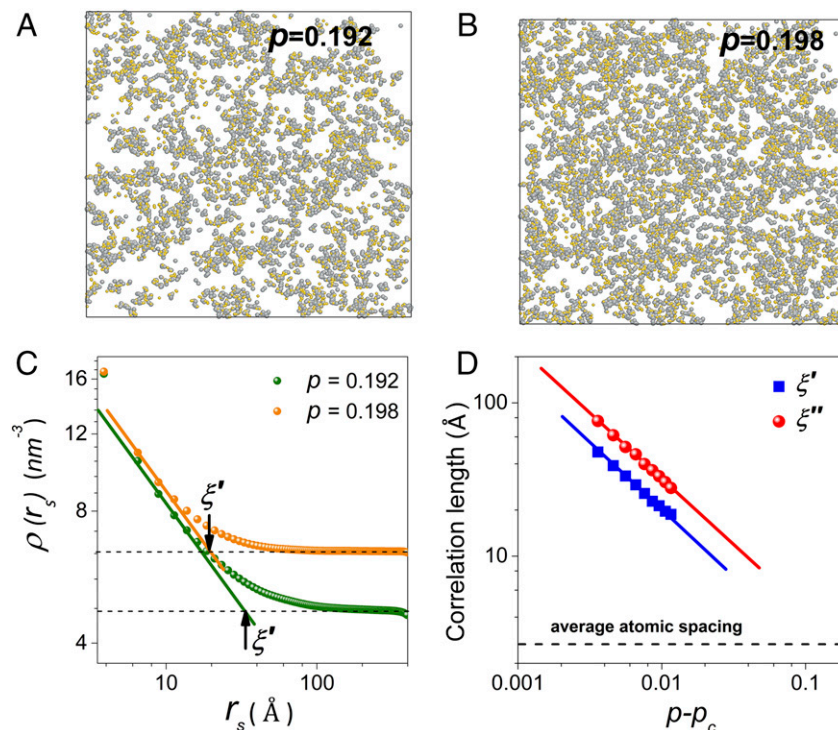


Fig. 2. Percolation clusters and their correlation length in MGs. For the $\text{Cu}_{46}\text{Zr}_{54}$ MG (large-scale sample with ~ 27 million atoms) at zero pressure, *A* and *B* are the atomic configurations of slices for percolation clusters with the occupation probability $p = 0.192$ and 0.198 , respectively; gray and yellow balls represent Zr and Cu atoms, respectively. (*C*) Average atomic density of percolation clusters, $\rho(r_s)$ vs. radial distance r_s for two corresponding values of occupation probability p ; the corresponding correlation lengths ξ' are denoted at the slope crossover. (*D*) Correlation lengths ξ' and ξ'' are plotted vs. $p - p_c$, where solid lines represent the best fit to Eq. 6, assuming $\nu = 0.875$. The dashed line indicates the average atomic spacing.

We consider next a similar fractal analysis for cluster packing in MGs, exploring the fractal model for packing of solute-centered clusters at medium-range scales (9). Fig. 1C shows a plot of the mass distribution analysis (Eq. 2) for the solute atoms, considering three typical MG samples studied by the MD simulations, for example, P-centered quasicivalent clusters in Ni₈₀P₂₀ MG (Fig. 1A). $M(r_s)$ in Fig. 1C represents the number of solute-centered clusters within r_s , obtained as the mass distribution of the solute atoms. Similar to the analysis in Fig. 1B, the scaling between $M(r_s)$ and normalized $r_s/r_{\text{ave_cluster}}$ for MGs collapse on a line with $D_f = 3$, as shown in Fig. 1C, provided r_s is normalized by the corresponding average cluster spacing $r_{\text{ave_cluster}} = (V_{\text{cluster}})^{1/3}$, where V_{cluster} is defined as the average volume of solute-centered clusters (i.e., the total volume of the MG sample divided by the number of solute-centered clusters). Hence the dimensionality $D_f = 3$ in Fig. 1C establishes that the solute atoms (reflecting the solute-centered clusters) in MGs are similarly not packed in a fractal network.

Collectively, the analyses presented above for the 12 samples obtained from MD simulation do not provide support for fractal scaling in the arrangement of either all of the atoms or solute-centered clusters in the MG structures studied. Only when a subgroup of atoms is considered (i.e., p significantly less than 1) do we find that the mass (or density of atoms) is spatially distributed according to fractal scaling as percolation clusters exhibiting correlation lengths at atomic scales.

Power-Law Scaling of $V \sim r^D$ or $(1/q)^D$

In light of these results above, it is important to consider in more detail the analyses in previous work that led to conclusions of fractal structuring based on measured noninteger powers $D \approx 2.5$ or 2.3 in the relations given in Eq. 1, through studies of the pressure- or composition-dependent peaks of RDFs and structure factors (8–10, 12). In particular, we make two important observations based on analyses of the current and previously published data that help to clarify the origin of the disparate conclusions.

First, the power D derived from analyses based on Eq. 1 cannot be relied upon to determine the fractal dimension of MGs. To illustrate the distinction between fractal structure and analyses based on Eq. 1, we consider the simple example of 2D Sierpinski gaskets (11). A 2D Sierpinski gasket is a classical non-random fractal with fractal dimension $D_f = \ln 3 / \ln 2 = 1.585$, which is illustrated in Fig. 3A and B for different values of the edge length (l) and homogeneous strain (ϵ), respectively. Shown in Fig. 3C with solid lines is the scaling of the density vs. the edge length (l), which exhibits the expected fractal scaling of $\rho(l) \sim l^{D_f-2} = l^{-0.415}$ (similar to the discussion in Fig. 1 and Fig. 2) at each homogeneous strain ϵ . The dashed lines in Fig. 3C connect points at similar levels for different values of ϵ , following the

analysis of Eq. 1; it is clear that the strain dependence displays a power-law behavior with an exponent of -2 (i.e., corresponding to the topological dimension). This latter power-law dependence with homogeneous strain (dashed lines) exhibits inverse scaling with the topological dimension, as expected for any material, fractal or nonfractal, glassy or crystalline, assuming homogeneous (or affine) deformation is applied (i.e., uniform scaling of the atomic coordinates according to the change of the sample dimensions). This point is reinforced by the analysis summarized in Fig. S4, where we examine the shift of the first-peak position in the RDF with pressure for a Cu₄₆Zr₅₄ MG (sample 2 in Table 1), under the constraint of imposed affine deformations; the results show that the peak position scales with the volume according to Eq. 1 with $D = 3$, as expected. Although MGs indeed undergo inhomogeneous deformation (see analysis below), Fig. 3 clearly illustrates the critical point that fractals are structures with repeating self-similar patterns at different length scales, and their characterization requires analysis of power-law scaling across a range of length scales, to establish the fractal dimension (e.g., analysis of Eq. 2). Such conclusions cannot be drawn solely from the analysis of the sample volume dependence of the peak positions of RDFs using Eq. 1.

Second, an analysis of the current results and previously published experimental data does not support the proposal (8, 9, 12–14) of a universal noncubic power D characterizing the scaling of Eq. 1 [i.e., $V \sim r^D$ or $(1/q)^D$, where $D \approx 2.5$ or 2.3] for MGs with varying compositions or pressure. We first consider the analysis of the pressure-dependent change in RDF peaks with sample volume, using the approach employed in ref. 8, for the MD simulation models of Cu₄₆Zr₅₄ and Ni₈₀Al₂₀ MGs. However, as shown in Fig. S5, we find that this noninteger power D cannot be reproduced even for Cu₄₆Zr₅₄ and Ni₈₀Al₂₀ MGs, and that the results for D are found to be highly sensitive to the method for measuring peak positions. Thus, in our current analysis, the RDFs are computed with finer resolution due to the larger MD simulations considered (Fig. S1). The results are shown in Fig. 4A for the scaling between $\ln(V_0/V)$ and $\ln(r_0/r)$ for all MGs in Table 1 under applied pressures. These results indicate that the values of D fluctuate between 2.5 and 4.0 (and can thus exceed 3), without any universal power-law scaling. The range of values for D in Fig. 4A can be mainly understood from two aspects: (i) The first-peak positions for the RDFs are not reliable estimates of the atomic neighbor-separation distances in binary or multicomponent MGs, because these peaks represent a superposition of partial pair distribution functions for different bond types with possibly large differences in bond lengths. For instance, in Fig. 5A, the shapes of first peak of the RDF for the Cu₄₆Zr₅₄ MG (sample 2) is irregular and the position of the maximum is mainly determined by Cu–Zr pairs rather than all pair types. (ii) Deformation

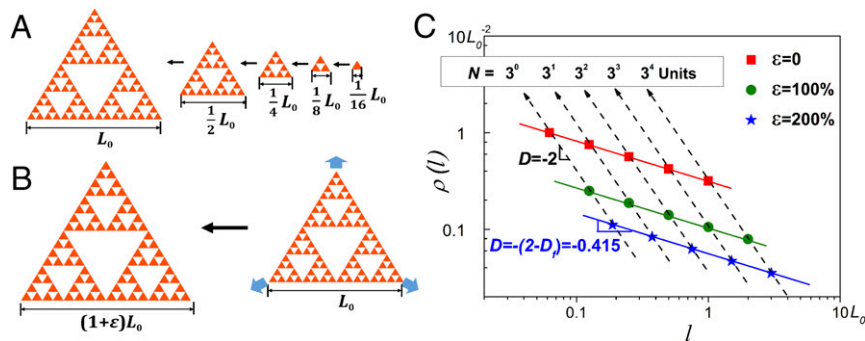


Fig. 3. Dimensionality of Sierpinski gaskets. (A) Typical Sierpinski gaskets at the first few stages in the aggregation with the denoted edge length l . (B) Description of stretched Sierpinski gasket at a strain ϵ . (C) Edge length (l)-dependent density $\rho(l)$ for Sierpinski gaskets at the strain $\epsilon = 0, 100\%, 200\%$; the solid lines indicate the power-law scaling with aggregation (with data at the same strain), and their slopes relate with the fractal dimension ($D_f = 1.585$) of Sierpinski gaskets; dashed lines reflect the scaling with stretching (with the same number of occupied triangle units, but at different strains).

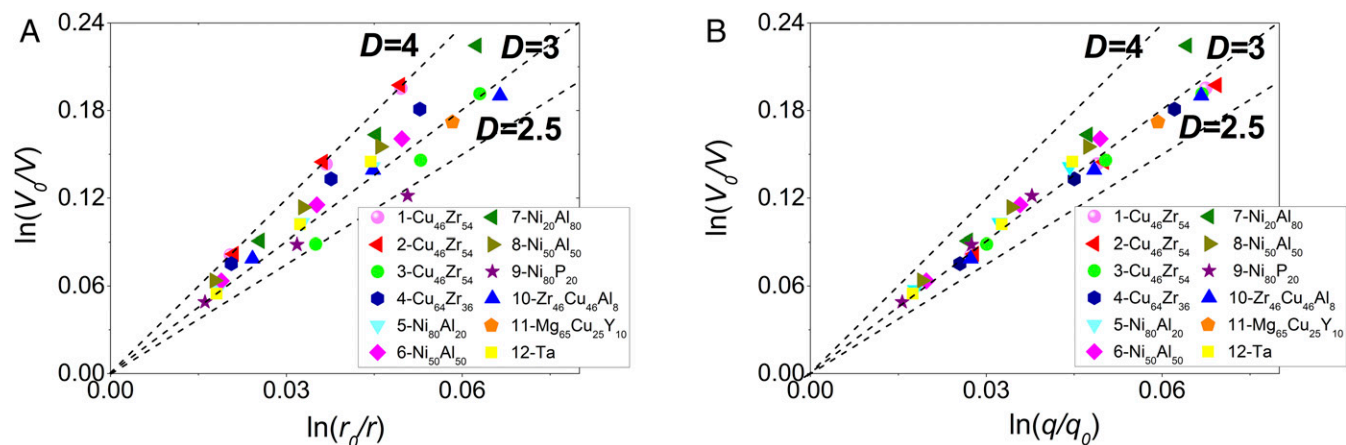


Fig. 4. Analysis of pressure-dependent RDFs and structure factors. (A) Scaling between $\ln(V_0/V)$ and $\ln(r_0/r)$ for all MGs in Table 1 at different applied pressures. In these plots, r and V are the first-peak positions of the RDFs and atomic volume, respectively (r_0 and V_0 correspond to pressure $P = 0$ GPa). The dashed lines represent several power-law scaling exponents D as denoted. (B) Scaling between $\ln(V_0/V)$ and $\ln(q/q_0)$ for all MGs in Table 1 at different applied pressures. q denotes the principal diffraction peak of simulated X-ray total structure factors ($q = q_0$ at $P = 0$ GPa).

in MGs is intrinsically inhomogeneous, because the different bond types display different compressibilities (7, 21, 22), such that the RDFs derived by summing the contributions of the partial pair distribution functions change shape and intensity with applied pressure, rather than simply scaling and rigidly shifting; this point is illustrated clearly in Fig. 5B, Fig. S6, and *SI Text*. Hence, in the scaling relation $V \sim r^D$, the exponent D does not necessarily equal 3. The essential point is that this observation does not directly imply a fractal structure. Furthermore, the exponent D derived from second, third, and fourth peak positions in $g(r)$ for all studied MGs are also included in Fig. S7. For each MG, D is observed to increase, decrease, or fluctuate with increasing peak positions, showing a general trend of convergence toward 3 at larger r .

For the analysis of the scaling of the principal diffraction peak q in the total structure factor via the relation of $V \sim (1/q)^D$, the situation is more complex, because the physical significance of q for MGs is not as well defined as it is for crystalline metals/alloys (as discussed in refs. 7, 15, 23, and 24). In particular, the interpretation of the principal diffraction peak q in multicomponent amorphous solids is complicated by the fact that the diffraction maximum is a sum of weighted partial functions with different atomic scattering factors (23, 25) (*SI Text*). In refs. 8, 9, 12–14, the value $D \approx 2.5$ or $D \approx 2.3$ have been measured for MGs, for the pressure and composition dependence of q obtained through X-ray diffraction. We investigated the universality of this result by simulating the X-ray total structure factor $S(q)$ for the MGs listed in Table 1 (*SI Text*). We first consider the analysis of $V \sim (1/q)^D$, where volume changes are induced by composition variations; our analysis summarized in Fig. S8 demonstrates the absence of a universal D for all of the MGs considered. Furthermore, Fig. 4B plots the scaling between $\ln(V_0/V)$ and $\ln(q/q_0)$ for all MGs studied at various hydrostatic pressure values, and the power D is observed to span values ranging between 2.8 and 3.6. The results from the current analysis thus do not support the universality of the scaling exponent D characterizing the relationship of $V \sim (1/q)^D$ for MGs under hydrostatic pressure and compositional variation.

Discussions and Conclusions

The central conclusion of the current work is that there is an absence of fractal structure related to the packing of all of the atoms or solute-centered clusters in MGs. This finding is consistent with the high packing fractions that characterize these materials, which are close to, or even exceeding, those of crystalline metals/alloys, with no noticeable pores at the atomic scale. Although the packing fractions for MGs and crystalline metals/

alloys are similar, they exhibit quite different structures as well as deformation behavior. Specifically, unlike crystalline materials, the structure of MGs is heterogeneous on the atomic scale, and their deformation nonaffine. These fundamental features of MG structures challenge the interpretation of the changes in the RDFs and structure factor peaks induced by pressure and compositional variations, as described above. The percolation analysis presented in the present work does reveal that a subgroup of atoms, drawn randomly from a MG structure, may show a fractal structure at small length scales as well as long-range homogeneous atomic packing, consistent with the behavior of a percolation cluster. This analysis helps to put MGs within the context of previous applications of percolation theory, including in crystalline metals/alloys. More importantly, our analysis of the percolation clusters within MGs, including their cluster structure and percolation threshold, may provide a powerful theoretical framework to describe the properties of amorphous alloys, such as the glass transition, shear banding/localization, and elasticity (26–29). It would be particularly interesting if the specific subgroup represents atoms with an extraordinary degree of icosahedral short-range order or high free volume. For instance, the glass transition and shear banding, that is, α processes in the potential energy landscape (30),

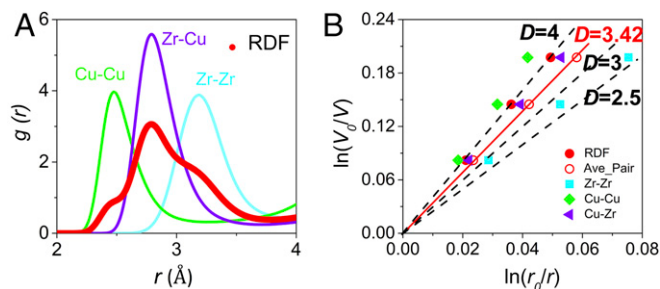


Fig. 5. Inhomogeneous deformation of MGs. (A) RDFs and partial pair distribution functions (pairs of Cu–Cu, Zr–Zr, and Cu–Zr) for the $\text{Cu}_{46}\text{Zr}_{54}$ MG (sample 2) at $P = 0$ GPa; the shape of first peak of the RDF is irregular, and the position of the maximum is mainly determined by Cu–Zr pairs rather than all pair types. (B) Scaling between $\ln(V_0/V)$ and $\ln(r_0/r)$ for the $\text{Cu}_{46}\text{Zr}_{54}$ MG (sample 2) at various applied pressures, where r denotes the positions of the first peak in the RDFs and the partial pair distribution functions (pairs of Cu–Cu, Zr–Zr, and Cu–Zr); different pairs exhibit different changes under hydrostatic pressure; note that red empty circles represent the weighted average summed over each pair of peaks, which exhibits a slope of $D \approx 3.42$.

are proposed as the percolation of free volume or liquid-like sites (26, 27). Also, the percolation of icosahedral short-range order has been demonstrated to form the backbone in some MGs, which would significantly determine their shear localization and elasticity (28, 29).

To conclude, we have conducted detailed fractal and percolation analyses of the structure of MGs samples, derived from computer simulations as well as from experimental data drawn from the literature. The significance of present work is threefold: (i) our systematic analyses demonstrate a lack of fractal nature considering the packing of all atoms or solute-centered clusters in MGs. This finding clarifies the long-standing debate over the packing structure of MGs from the perspective of fractal models. Specifically, the packing of atoms in MGs is demonstrated to be nonfractal, in contrast with previous conclusions drawn mainly from analyses of pressure (or composition) induced changes of RDF and structure factor peak positions using Eq. 1 (8, 9, 12). This contradiction results from the assumed connection between the scaling in Eq. 1 and the fractal distribution of the atomic mass/density, which has been demonstrated to be not generally valid. It is worth emphasizing again that fractals are structures with repeating self-similar patterns at different length-scales; identifying their presence thus requires analysis spanning a range of length scales to accurately characterize their dimension. (ii) For MGs, the shift of RDF and structure factor peaks, induced by pressure or compositional variations, result from their intrinsic heterogeneous structure as well as nonaffine deformations. The power D in Eq. 1 is demonstrated to be non-universal and can even exceed 3, as it depends on the details of the structure and bonding in a specific system. (iii) Our work presents detailed analyses of MG structures using concepts from percolation theory, which have been proposed to relate with key properties, including the glass transition and mechanical deformation. Therefore, such studies help pave the way toward the fundamental

and concrete understanding of the atomic-level structure as well as structure–property relationships in MGs.

Methods

Sample Preparation. Large-scale MD simulations were implemented to study 12 different model MGs as listed in Table 1. The MG systems were prepared by quenching from the melt, with a range of cooling rates (10^{10} to 10^{13} K/s). Samples 2, 3, and 5 are the same as the systems $\text{Cu}_{46}\text{Zr}_{54}$ (FF1), $\text{Cu}_{46}\text{Zr}_{54}$ (FF2), and $\text{Ni}_{80}\text{Al}_{20}$, respectively, studied in ref. 8, but in the present work larger simulation boxes containing more than 1 million atoms were used. Hydrostatic pressures of 0, 10, 20, and 30 GPa, respectively, were applied to each MG sample. The pressure was ramped up at a rate of 10 GPa/ns. At each desired pressure, the MG was relaxed at 300 K for up to 2.0 ns with 100 configurations sampled over additional 0.1-ns simulations. These 100 atomic configurations were used to calculate the RDF for each MG sample. The resolution (i.e., the bin size) of these RDFs was 0.005 Å (Fig. S1).

Percolation Analysis. Within each MG system, 1,000 independent samples were generated by randomly selecting a subgroup of atoms for each of the occupation probabilities p considered. More details related to the method of percolation analysis can be found in refs. 19 and 20. Our percolation analysis (leading to the results shown in Fig. 2 and Fig. S3) of MG structures was performed on large-scale samples (with ~ 27 million atoms) to reduce any finite scaling effects, which are generated by replication with a $3 \times 3 \times 3$ array. The percolation threshold p_c is evaluated as the critical occupation probability for forming percolation clusters. The nearest-neighbor atoms for the MGs are determined as the atoms within the distance corresponding to the first minimum of the RDF (Fig. S1).

ACKNOWLEDGMENTS. We thank Prof. Evan Ma and Drs. Yongqiang Cheng and Ashvini Shekhawat for their thoughtful discussions. This work was supported by the Mechanical Behavior of Materials Program (KC13) at the Lawrence Berkeley National Laboratory, funded by the US Department of Energy, Office of Science, Office of Basic Energy Sciences, Materials Sciences and Engineering Division, under Contract DE-AC02-05CH11231. The study made use of resources of the National Energy Research Scientific Computing Center, which is also supported by the Office of Basic Energy Sciences of the US Department of Energy under Contract DE-AC02-05CH11231.

- Greer AL (2014) Metallic glasses. *Physical Metallurgy*, eds Laughlin DE, Hono K (Elsevier, Amsterdam), 5th Ed, pp 305–385.
- Schroers J (2013) Bulk metallic glasses. *Phys Today* 66:32–37.
- Schuh CA, Hufnagel TC, Ramamurty U (2007) Mechanical behavior of amorphous alloys. *Acta Mater* 55:4067–4109.
- Demetriou MD, et al. (2011) A damage-tolerant glass. *Nat Mater* 10:123–128.
- Miracle DB (2004) A structural model for metallic glasses. *Nat Mater* 3:697–702.
- Sheng HW, Luo WK, Alamgir FM, Bai JM, Ma E (2006) Atomic packing and short-to-medium-range order in metallic glasses. *Nature* 439:419–425.
- Cheng YQ, Ma E (2011) Atomic-level structure and structure–property relationship in metallic glasses. *Prog Mater Sci* 56:379–473.
- Chen DZ, et al. (2015) Fractal atomic-level percolation in metallic glasses. *Science* 349:1306–1310.
- Ma D, Stoica AD, Wang XL (2009) Power-law scaling and fractal nature of medium-range order in metallic glasses. *Nat Mater* 8:30–34.
- Chen DZ, An Q, Goddard WG, III, Greer JR (2016) Ordering and dimensional crossovers in metallic glasses and liquids. *Phys Rev B* 95:024103.
- Bunde A, Havlin S (1996) *Fractals and Disordered Systems* (Springer, New York), 2nd Ed.
- Zeng Q, et al. (2016) General 2.5 power law of metallic glasses. *Proc Natl Acad Sci USA* 113:1714–1718.
- Zeng Q, et al. (2014) Universal fractional noncubic power law for density of metallic glasses. *Phys Rev Lett* 112:185502.
- Gangopadhyay AK, et al. (2014) Thermal expansion measurements by x-ray scattering and breakdown of Ehrenfest's relation in alloy liquids. *Appl Phys Lett* 104:191907.
- Mattern N (2014) Comment on "Thermal expansion measurements by x-ray scattering and breakdown of Ehrenfest's relation in alloy liquids." *Appl Phys Lett* 105:256101.
- Allen MP, Tildesley DJ (1987) *Computer Simulation of Liquids* (Clarendon, Oxford).
- Falconer K (2004) *Fractal Geometry: Mathematical Foundations and Applications* (Wiley, Chichester, UK).
- Mendelev MI, et al. (2009) Development of suitable interatomic potentials for simulation of liquid and amorphous Cu–Zr alloys. *Philos Mag* 89:967–987.
- Stauffer D, Aharony A (1994) *Introduction to Percolation Theory* (CRC Press, Boca Raton, FL).
- Kapitulnik A, Aharony A, Deutscher G, Stauffer D (1983) Self similarity and correlations in percolation. *J Phys Math Gen* 16:L269–L274.
- Sheng HW, Ma E, Liu HZ, Wen J (2006) Pressure tunes atomic packing in metallic glass. *Appl Phys Lett* 88:171906.
- Ketov SV, et al. (2015) Rejuvenation of metallic glasses by non-affine thermal strain. *Nature* 524:200–203.
- Warren BE (1969) *X-Ray Diffraction* (Courier Corporation, New York).
- Freltoft T, Kjems JK, Sinha SK (1986) Power-law correlations and finite-size effects in silica particle aggregates studied by small-angle neutron scattering. *Phys Rev B Condens Matter* 33:269–275.
- Sheng HW, et al. (2007) Polymorphism in a metallic glass. *Nat Mater* 6:192–197.
- Cohen MH, Grest G (1979) Liquid-glass transition, a free-volume approach. *Phys Rev B* 20:1077.
- Greer AL, Cheng YQ, Ma E (2013) Shear bands in metallic glasses. *Mater Sci Eng Rep* 74:71–132.
- Shi Y, Falk ML (2005) Strain localization and percolation of stable structure in amorphous solids. *Phys Rev Lett* 95:095502.
- Ding J, Cheng YQ, Ma E (2014) Full icosahedra dominate local order in $\text{Cu}_{64}\text{Zr}_{36}$ metallic glass and supercooled liquid. *Acta Mater* 69:343–354.
- Debenedetti PG, Stillinger FH (2001) Supercooled liquids and the glass transition. *Nature* 410:259–267.
- Cheng YQ, Ma E, Sheng HW (2009) Atomic level structure in multicomponent bulk metallic glass. *Phys Rev Lett* 102:245501.
- Pun GPP, Mishin Y (2009) Development of an interatomic potential for the Ni–Al system. *Philos Mag* 89:3245–3267.
- Mishin Y, Mehl MJ, Papaconstantopoulos DA (2002) Embedded-atom potential for B2 – NiAl. *Phys Rev B* 65:224114.
- Sheng HW, Ma E, Kramer MJ (2012) Relating dynamic properties to atomic structure in metallic glasses. *JOM* 64:856–881.
- Ding J, Cheng YQ, Ma E (2013) Charge-transfer-enhanced prism-type local order in amorphous $\text{Mg}_{65}\text{Cu}_{25}\text{Y}_{10}$: Short-to-medium-range structural evolution underlying liquid fragility and heat capacity. *Acta Mater* 61:3130–3140.
- Zhong L, Wang J, Sheng H, Zhang Z, Mao SX (2014) Formation of monatomic metallic glasses through ultrafast liquid quenching. *Nature* 512:177–180.
- Mattern N, et al. (2003) Structural behavior of $\text{Pd}_{40}\text{Cu}_{30}\text{Ni}_{10}\text{P}_{20}$ bulk metallic glass below and above the glass transition. *Appl Phys Lett* 82:2589–2591.
- Hsieh HY, et al. (1990) Atomic structure of amorphous $\text{Al}_{90}\text{Fe}_x\text{Ce}_{10-x}$. *J Mater Res* 5:2807–2812.